Temperature transformation of blended magnesium potassium phosphate cement binders

Laura J. Gardner [a], Sam A. Walling [a], Claire L. Corkhill [a], Susan A. Bernal [a,1], Valentin Lejeune [a,b], Martin C. Stennett [a], John L. Provis [a], Neil C. Hyatt [a,*]

[a] Department of Materials Science and Engineering, University of Sheffield, Sheffield S1 3JD, UK
[b] École Nationale Supérieure de Chimie de Montpellier, 34090 Montpellier, France

A B S T R A C T

In this study, a multi-technique approach was utilised to determine the high temperature performance of magnesium potassium phosphate cement (MKPC) blended with fly ash (FA) or ground granulated blast furnace slag (GBFS) with respect to nuclear waste immobilisation applications. Conceptual fire conditions were employed (up to 1200 °C, 30 min) to simulate scenarios that could occur during interim storage, transportation or within a final geological disposal facility. After exposure up to 400 °C, the main crystalline phase, struvite-K (MgKPO$_4$·6H$_2$O), was dehydrated to poorly crystalline MgKPO$_4$ (with corresponding volumetric and mass changes), with MgKPO$_4$ recrystallisation achieved by 800 °C. XRD and SEM/EDX analysis revealed reaction occurred between the MgKPO$_4$ and FA/GBFS components after exposure to 1000–1200 °C, with the formation of potassium aluminosilicate phases, leucite and kalsilite (KAlSi$_2$O$_6$ and KAlSiO$_4$), commensurate with a reduced relative intensity (or complete elimination) of the dehydrated struvite-K phase, MgKPO$_4$. This was further supported by solid-state NMR (^{27}Al and ^{29}Si MAS), where only residual features associated with the raw FA/GBFS components were observable at 1200 °C. The high temperature phase transformation of blended MKPC binders resulted in the development of a glass/ceramic matrix with all existing porosity infilled via sintering and the formation of a vitreous phase, whilst the physical integrity was retained (no cracking or spalling). This study demonstrates that, based on small-scaled specimens, blended MKPC binders should perform satisfactorily under fire performance parameters relevant to the operation of a geological disposal facility, up to at least 1200 °C.

1. Introduction

Cementitious binders based on magnesium potassium phosphate (MKPC) bonding are, in general, near-neutral pH systems formed from the acid-base reaction of KH$_2$PO$_4$ and dead burnt MgO [1,2]. The resulting hydrous, strength-giving mineral, struvite-K (MgKPO$_4$·6H$_2$O), is the main binding phase in these cements (Eq. (1)). MKPCs benefit from a near-neutral pH, low drying shrinkage, low demand for water during mixing and high compressive strengths from early ages [2–4], compared to other cementitious systems. These properties have led to consideration of MKPCs as encapsulants/grouts for the stabilisation of nuclear wastes, including (but not limited to): the physical encapsulation of plutonium contaminated ashes [5], liquid wastes [2,6] and the immobilisation of cesium (accommodated within struvite-K by partial K

replacement) [7]. The latter is achievable via the affinity of the struvite mineral group to include NH$_4^+$, K$^+$, Cs$^+$, TI$^+$ or Rb$^+$ cations within the structure [8]. Of particular interest is the encapsulation of reactive metals (Al, Mg and U), which may corrode in the high pH, conditions or high availability of free water, present within conventional Portland cement (PC) based encapsulants [9–13]. The impact of reactive metal corrosion could be problematic from two aspects, firstly, the formation of expansive products (e.g. U$_{(s)}$ + 2H$_2$O$_{(l)}$ → UO$_2$$_{(s)}$ + H$_2$$_{(g)}$), which results in a volumetric change within the wasteform and has potential to lead to stress-induced fractures [14]. Secondly, the concurrent production of hydrogen gas presents a flammability hazard during interim storage, transportation and disposal scenarios. The corrosion reaction products both have potential to cause pressurisation and distortion of the waste container [15], which is undesirable from a long-term safety

aspect.

$$MgO_{(s)} + KH_2PO_{4\,(s)} + 5H_2O_{(l)} \rightarrow MgKPO_4 \cdot 6H_2O_{(s)} \qquad (1)$$

The acceptance of a conditioned nuclear wasteform and waste package is contingent on meeting the safety requirements laid out in waste package specifications and acceptance criteria. In the United Kingdom (UK), these requirements pertain to the mechanical, thermal and immersion properties of the wasteforms and waste packages [16,17]. The thermal properties of waste packages are especially important for understanding and assessing the potential impact of accident scenarios, such as fires, which might occur during transportation, or after emplacement of a waste package into an engineered repository (either for temporary or final storage). It is imperative that waste packages, as the primary engineered barrier, minimise the release of radioactive material under such fire conditions, which may burn hotter, and for longer due to limited access, especially if deep underground in a geological disposal facility [16]. This is especially pertinent in light of the recent fires and subsequent radionuclide release at the Waste Isolation Pilot Plant (WIPP), United States of America (USA) in 2014 [18], which highlights the importance of understanding how waste packages might evolve and behave at elevated temperatures.

Typically, upon heating, cementitious materials undergo dehydration and breakdown of the principal binding phases, which leads to water evaporation and the build-up of pressure within the pores [19,20]. As a consequence of the internal stresses generated by differential thermal expansion and shrinkage, in addition to the water evaporation, severe loss of mechanical performance is experienced; for example, a blended blast furnace slag/Portland cement (1:1) mortar exposed to 900 °C for 4 h exhibited a strength loss of ~84% compared to the initial strength at 20 °C (30 MPa) [19].

Magnesium phosphate compounds historically found use as refractory materials around high temperature furnaces [21–24], whilst current MKPC interests have evolved to include fire-retardant coatings or composites due to high level of fire resistance [25,26]. Hence, it is anticipated that MKPCs should be capable of withstanding a wide range of temperature conditions within the remit of waste management accident scenarios. Most of the literature regarding the thermal properties of magnesium phosphate cements is based upon magnesium ammonium phosphate cements ($NH_4MgPO_4 \cdot 6H_2O$; struvite; MAP) rather than MKPC binders, which are now the preferred ammonium-free binders. Within ammonium-containing systems, various phase transitions were identified upon heating due to liberation of both the crystal-bound H_2O and NH_3 above 50 °C, resulting in intermediate poorly crystalline magnesium phosphates [27,28], and leading ultimately to the sintering of ceramic-like $Mg_3(PO_4)_2$ at 1300 °C [28].

In practical cementitious applications, MKPC binders are often blended up to 50 wt% replacement with fly ash (or other fillers, *e.g.* metakaolin, silica fume) to minimise the exothermic output of the acid-base reaction, improve compressive strength, reduce material costs, ensure sufficient workability and improve water resistance [4,12,29,30]. A study on blended MKPCs (up to 40 wt% fly ash) reported the conversion of struvite-K ($MgKPO_4 \cdot 6H_2O$) to $MgKPO_4$ [31] when exposed to 1000 °C for 3 h. These cements retained ~28% of their original compressive strength (76.7 MPa), with the conclusion that fly ash was detrimental to the high temperature resistance of MKPC [31]. Whilst the addition of wollastonite, $CaSiO_3$, (at 5–10 mol% of the MgO content) was shown to improve the physical and mechanical integrity of MKPC when exposed up to 1000 °C, however, K was eliminated from the phase assemblage [32] similar to MAP systems, which undergo NH_3 liberation >50 °C [27,28]. Preliminary studies of MKPC binders blended with 50 wt% fly ash (FA/MKPC) and ground granulated blast furnace slag (GBFS/MKPC) showed that a disordered $MgKPO_4$ phase was formed upon heating to 200 °C, followed by crystallisation of K-bearing phases at temperatures below 1000 °C [33]. It is therefore important to further understand the impact of fillers on the physical and chemical stability of blended MKPC binder after exposure to high temperatures.

In this study, MKPC binders blended with fly ash and ground granulated blast furnace slag were exposed to temperatures between 20 °C to 1200 °C. The resulting products were characterised using dilatometry, X-ray diffraction (XRD), scanning electron microscopy (SEM), solid state magic angle spinning (MAS) nuclear magnetic resonance (NMR) techniques ([27]Al and [29]Si), and Mössbauer spectroscopy. Here, we discuss the microstructural stability of these MKPC materials exposed to high temperatures to elucidate the possible failure mechanisms in potential fire scenarios relevant to a geological disposal facility.

2. Experimental methodology

2.1. Materials

The cementitious binder precursors were: dead burnt magnesium oxide (MgO; 89% purity; RBH Ltd), potassium dihydrogen phosphate (KH_2PO_4; Prayon; KDP) available as Food Grade E340 MKP (>99% purity), and boric acid (H_3BO_3; >99.5% purity; Fisher Scientific). Fly ash (FA) was supplied by CEMEX as BS EN 450-1 S [34]. Ground granulated blast furnace slag (GBFS) was supplied by Hanson Cements (from Scunthorpe works) in accordance with established Sellafield Limited specifications for the UK nuclear industry. It is a blend of fine slag and coarse ground material (calumite) of the same composition at a 2:1 ratio. Detailed characterisation of this slag blend is reported by Sanderson et al., [35]. The powder properties (Table 1) and chemical compositions of MgO, FA and GBFS were determined by X-ray fluorescence (XRF) oxide analysis (Table 2).

2.2. Mix procedure

The blended MKPC formulations (Table 3) were based on a MgO: KH_2PO_4 molar ratio of 1.7:1, and 50 wt% addition of FA or GBFS with a water-to-total-solids (w/s) ratio of 0.24, consistent with previous formulations [36]. A 2 wt% addition of H_3BO_3 was included as a set retarder, which resulted in a final setting time of 7 h and 6 h for FA/ MKPC and GBFS/MKPC, respectively. The precursors (MgO, KH_2PO_4, FA or GBFS, H_2O and H_3BO_3) were mixed initially for 10 min in a Kenwood mixer. Afterwards, the paste was transferred to a high shear Silverson L4RT mixer (4000 rpm) and mixed for 10 min to achieve a homogenous paste. The formulation design and mixing regime utilised in this study is consistent with UK-based MKPC research targeting nuclear waste applications [11,12,36,37]. Prior to thermal exposure, the binders were cured in an environmental chamber (20 °C, 95% relative humidity) in sealed vessels for 7 days.

2.3. Thermal test procedure

Blended MKPC samples were cut into cylinders (h = 10 mm ± 0.1

Table 1
Characterisation of raw materials using PSD, Blaine fineness, and BET surface area.

Material	d_{10} (μm)	d_{50} (μm)	d_{90} (μm)	Blaine fineness (m^2/kg)	BET S.A. (m^2/kg)
MgO	3.2 ± 0.1	24.4 ± 0.3	63.8 ± 0.6	329 ± 16	563 ± 72
KH_2PO_4	250 ± 1.5	600 ± 4.9	1210 ± 16.5	n.d.	n.d.
FA	2.7 ± 0.1	14.0 ± 0.3	66.1 ± 3.5	560 ± 10	2258 ± 10
BFS	1.6 ± 0.1	16.0 ± 0.1	1465 ± 15	497 ± 17	993 ± 72

Table 2
XRF oxide analysis of raw materials; MgO, FA and GBFS (precision ± 0.1 wt%).

Compound (wt%)	MgO	FA	GBFS
Na_2O	<0.1	1.1	0.4
MgO	88.9	1.7	7.9
Al_2O_3	1.7	25.2	12.0
SiO_2	4.3	50.2	36.6
P_2O_5	<0.1	0.3	<0.1
K_2O	0.1	3.6	0.7
CaO	2.1	2.4	40.2
Fe_2O_3	1.5	9.3	0.4
Total	98.8	93.8	98.3

Table 3
Formulation of blended MKPC binders produced with w/s = 0.24, based on a 500 g batch size to ±0.1 g precision.

Blend	MgO (g)	KH_2PO_4 (g)	H_2O (g)	FA (g)	GBFS (g)	H_3BO_3 (g)
FA/MKPC	77.8	154.6	96.0	165.0	–	6.6
GBFS/ MKPC	77.8	154.6	96.0	–	165.0	6.6

mm and d = 14 mm ± 0.5 mm) using a Buehler Isomet low speed saw. Using a zirconia tile, the samples were placed into a pre-heated furnace (Elite; model 15/5) at 400, 800, 1000 and 1200 °C ± 10 °C, respectively. After allowing time for the furnace to stabilize (<5 min) and a 30-min thermal exposure, the samples were removed and air-cooled to room temperature, as illustrated in Fig. 1. Sample dimensions were measured using digital callipers, and samples were weighed before and after high temperature exposure.

The thermal test methodology used in this study was complementary to both the International Atomic Energy Agency (IAEA) transport regulations [38] and the Radioactive Waste Management Limited (RWM) guidelines for a geological disposal facility (GDF) in the UK [16], which are based on full-scale wasteforms. The former requires samples to be fully engulfed at an average temperature of 800 °C (which is based on a hydrocarbon fuel fire with a flame emissivity coefficient of 0.9) for a 30

minute period [38], whereas the RWM parameters increased both the average temperature and exposure time to 1000 °C and 1 h, respectively [16]. The enhanced RWM parameters are intended to take into account the higher potential risk factor associated with fire incidents in a GDF, which may reach higher temperatures due to both radiated heat (e.g. from the fire) and heat reflected off tunnel features [16]. However, it is not expected that the entirety of a wasteform will be exposed to the maximum temperature. This is due to the low conductivity of PC-based grouts, which will reduce heat transfer from the external surface to the bulk internal region [16]. Large-scale testing and modelling using simulant wasteforms (500 L grouted drum; h = 1230 mm, d = 800 mm) revealed that only the initial 50 mm of the wasteform was exposed to high temperature during a 1-hour engulfed fire test, with the internal temperature below 150 °C. Therefore, the duration used in this study for relatively small sample sizes was considered appropriate, and also likely represents a worst-case scenario where a higher fraction of the grout was exposed to high temperature.

2.4. Analytical techniques

Dilatometry was utilised to determine the *in-situ* linear thermal expansion of FA/MKPC and GBFS/MKPC binders up to 1200 °C. Dilatometry was performed in a horizontal configuration using a NETZSCH DIL 402C dilatometer between 20 and 1200 °C at 10 °C/min under a constant 50 mN load in air (1 mL/min) on cylindrical samples of 8.5 ± 0.1 mm (diameter) and 5.7 ± 0.2 mm (length). The linear dimension changes, ΔL, were recorded as a function of temperature and expressed as a percentage of the initial length, L_0. The following analytical techniques were performed on samples after high temperature exposure and air-cooling to room temperature (. *i.e. ex-situ*). Powder X-ray diffraction (XRD) data were collected between $10° < 2\theta < 50°$ using a Bruker D2 PHASER desktop diffractometer with Ni filtered Cu Kα radiation (1.5418 Å) operating in reflection mode, using a step size of 0.02° and time per step of 1 s. Thermal analysis was conducted using a Perkin Elmer DTA 7 instrument, in alumina crucibles under a N_2 atmosphere at 10 °C/min, up to 1000 °C. Blended MKPC samples were polished and carbon coated for SEM analysis, which was performed using a low vacuum Hitachi TM3030 analytical benchtop SEM with an integrated Bruker Quantax 70 EDX (energy dispersive X-ray spectrometer) system
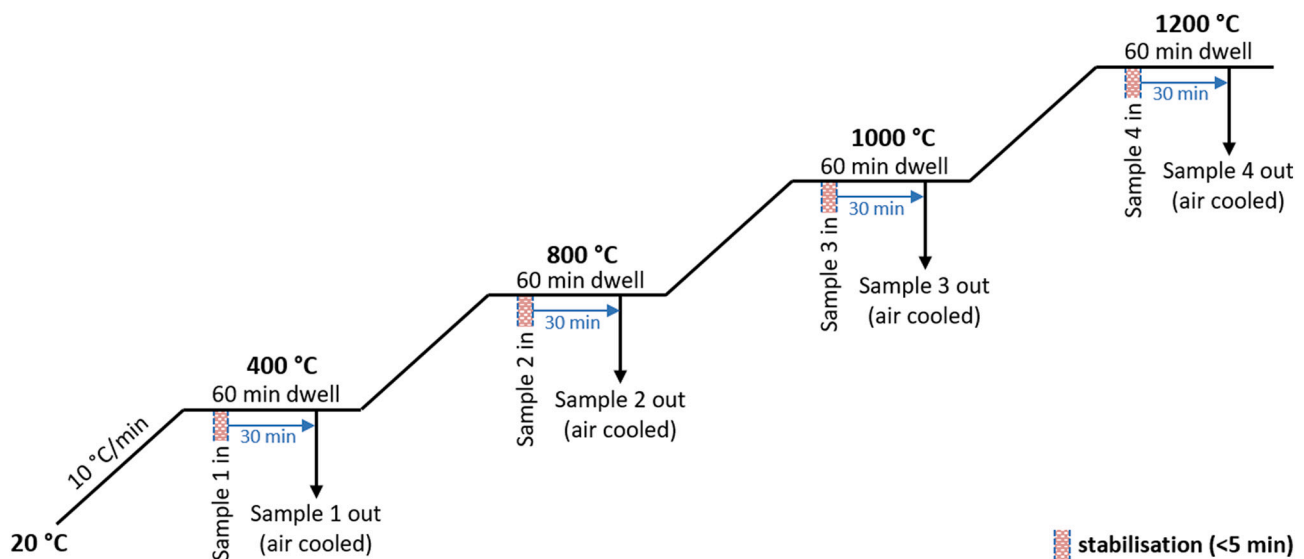

Fig. 1. Fire performance thermal treatment procedure.

at 15 kV and a 7.0 mm working distance. Mössbauer spectroscopy was conducted on a Wissel spectrometer (50 Ci ^{57}Co(Rh) source) using 512 channels and an Fe foil for calibration. Unique Fe species were assigned by fitting Lorentzian doublet and sextets using Recoil software [39].

Solid-state NMR spectra were collected on a Varian VNMRS 400 (9.4 T) spectrometer using zirconia rotors with a 4 mm o.d. probe for ^{27}Al nuclei and 6 mm o.d. probe for ^{29}Si nuclei. ^{27}Al MAS NMR spectra were collected at 104.198 MHz and a spinning speed of 14 kHz, employing a pulse width of 1 μs (25°), a relaxation delay of 0.2 s, and with 1500–7000 scans. The ^{29}Si MAS NMR spectra were collected at 79.435 MHz at a spinning speed of 6.8 kHz, and employed a pulse duration of 6.2 μs (90°) and a relaxation delay of 1.0–5.0 s, with between 1660 and 54,160 scans. ^{27}Al and ^{29}Si chemical shifts are referenced to external samples of 1.0 M aqueous Al(NO$_3$)$_3$ and tetramethylsilane (TMS), respectively.

3. Results and discussion

3.1. Physical properties

In Fig. 2, the photographs of the FA/MKPC and GBFS/MKPC binders after exposure to 400–1200 °C indicate that no visible spalling or cracking occurred as a result of high temperatures, which suggests these binders can withstand thermal test conditions without detrimental physical effects (with respect to small scale specimens). In the FA/MKPC binder (Fig. 2A), a progressive colour change (from dark grey *via* red-brown to a final dark brown) was observed between 20 °C (control) and >800 °C, which was thought to be associated with iron oxidation in the fly ash; this is examined in more detail below using Mössbauer spectroscopy (Section 3.5). Further to this, phase assemblage changes were expected following exposure to high exposures, which will be explored in the subsequent sections. In the GBFS/MKPC binder (Fig. 2B), a more subtle colour change (from grey to light grey) was observed, and the green tinge observed after low temperature exposure (200 °C) was attributed to polysulfide species released by the GBFS [40]. This faded
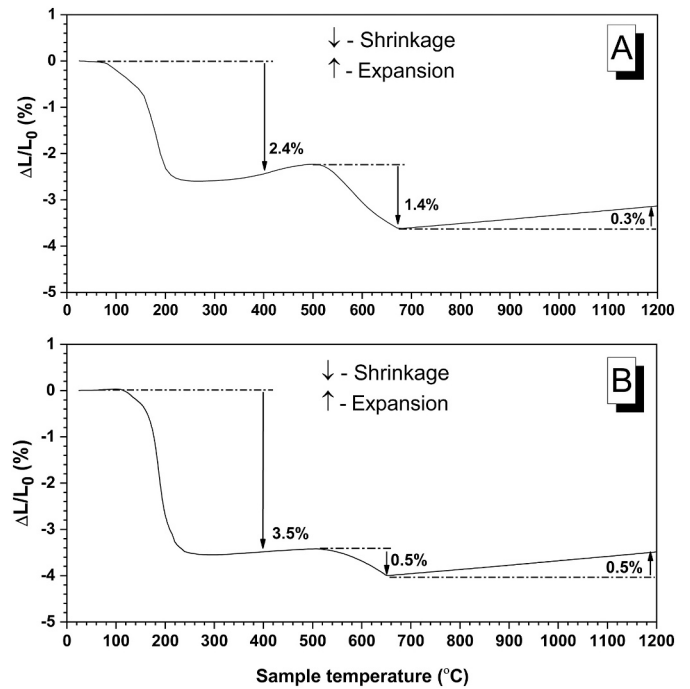

Fig. 3. *In-situ* dilatometric traces of the A) FA/MKPC and B) GBFS/MKPC binders.

with increasing temperatures and became indistinguishable after exposure to 1200 °C, where the sample was observed to be more porous than at all other temperatures. This physical change was associated with mass loss rather than volume expansion (Table 3).

The dimensional changes of the FA/MKPC and GBFS/MKPC binders were measured both *in-situ* (by dilatometry, Fig. 3) and *ex-situ* (using a digital micrometer, Table 4) to determine the effect of exposure to high
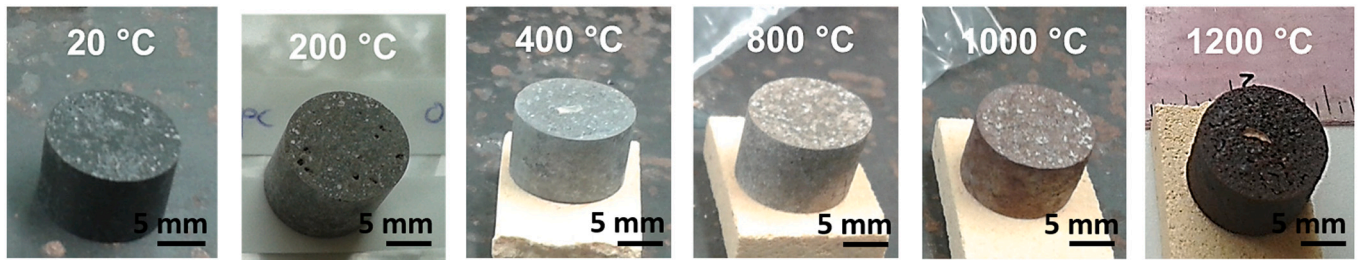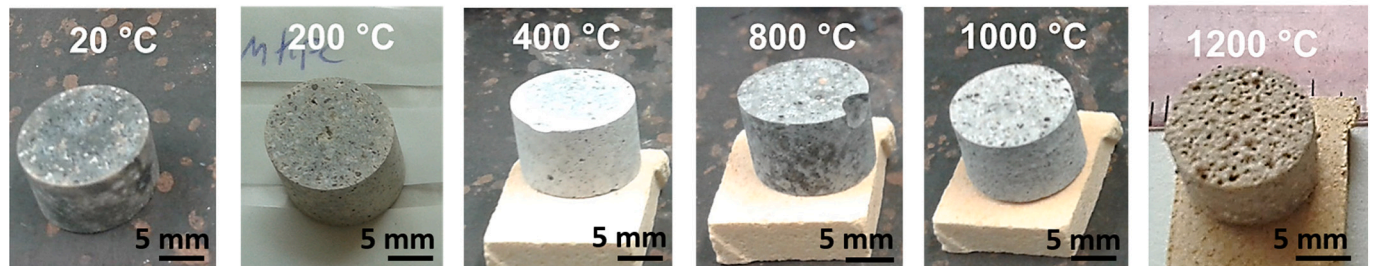

Fig. 2. Photographs of A) FA/MKPC and B) GBFS/MKPC hardened binders after exposure to temperatures between 20 °C and 1200 °C.

Table 4

The volumetric and mass changes of FA/MKPC and GBFS/MKPC binders exposed to high temperatures.

Temperature (°C)	% change after heating[b]			
	FA/MKPC		GBFS/MKPC	
	Volume ($\pm0.4\%$[a])	Mass ($\pm0.3\%$[a])	Volume ($\pm0.4\%$[a])	Mass ($\pm0.3\%$[a])
400	−6.3	−23.2	−8.6	−23.5
800	−7.9	−26.3	−8.0	−24.0
1000	−4.2	−26.4	−3.4	−23.7
1200	−1.2	−29.2	−0.6	−28.2

[a] The errors are associated with calculated standard deviations from the 800 °C experiment which was performed in triplicate.

[b] The percentage change on heating was calculated compared to the sample at 20 °C prior to heat treatment.

temperatures (400–1200 °C). The volumetric change (ΔV) was calculated from the initial cylindrical volume (V_0) at 20 °C and the final cylindrical volume (V_f) post-heat treatment, with the difference expressed as a percentage based on the initial volume ($\Delta V/V_0$), which is reported in Table 4.

According to Fig. 3, the principal mass loss event occurred after exposure to <200 °C, which was associated with the dehydration of struvite-K [29,41–43] and resulted in a mass change of ~−23% at 400 °C (the lowest temperature tested in the stepwise heating profile; Table 4) consistent with previous work [33]. At 400 °C, volumetric contractions of 6.3% (FA/MKPC) and 8.6% (GBFS/MKPC) were observed in the *ex-situ* measurements. The volumetric contraction observed at 400 °C in Fig. 3 was calculated to be 7.0% and 10.1% for FA/MKPC and GBFS/MKPC, respectively, which were broadly comparable to the *ex-situ* measurements (Table 4). This indicates that the differing heat profiles utilised during the *in-situ* (thermal contact with a cylindrical face) and *ex-situ* (fully exposed) methods resulted in similar dimensional changes. The dilatometry volume changes (ΔV) were converted from the observed linear dimension changes ($L_\%$) in Fig. 3, with the assumption that volume contraction occurred uniformly. As an example, FA/MKPC at 400 °C (2.4 $L_\%$; Fig. 3), could be represented by $\Delta V = (V_0 - (V_0 - L_\%))^3$, where the initial volume (V_0) is given an arbitrary value, *e.g.* $(1 - (1 - 0.024)^3 = 7.0\%$.

The maximum shrinkage was observed around 660 °C, which was equivalent a volumetric contraction of 10.4% (670 °C) and 11.5% (650 °C) for FA/MKPC and GBFS/MKPC, respectively, whilst a small thermal expansion was noted in the *in-situ* dilatometric tests of both binders between 700 and 1200 °C (Fig. 3). This was attributed to the formation of additional crystalline phases *via* the reaction of the supplementary cementitious materials (FA, GBFS) and the dehydrated struvite-K product (MgKPO₄), which was identified in the XRD analysis for both blended binders after exposure to >800 °C (discussed in detail in Section 3.2). Overall, the dilatometric samples experienced a total linear shrinkage of ~3.5% (equivalent to a volume contraction of ~10%), importantly the impact of this shrinkage did not result in cracking on spalling. This is encouraging from a fire performance aspect, as it indicated that both the FA/MKPC and GBFS/MKPC binders physically withstood exposure to high temperatures.

3.2. Powder X-ray diffraction

3.2.1. FA/MKPC

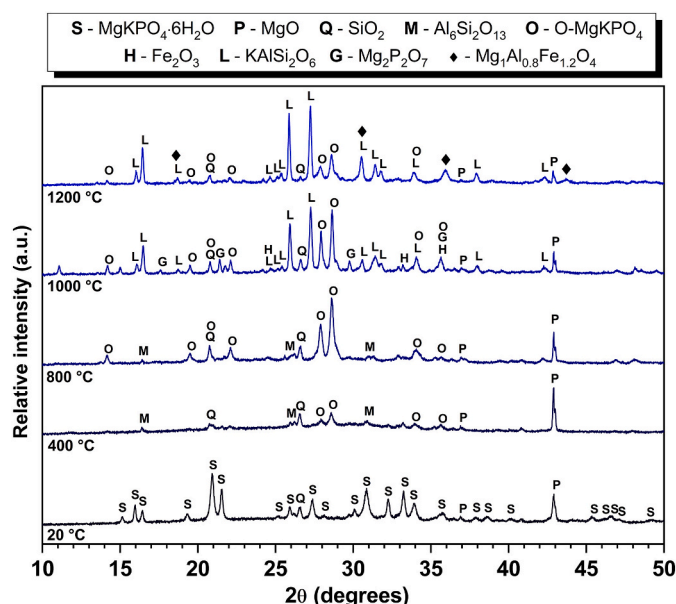At 20 °C, struvite-K (MgKPO₄·6H₂O, (Powder diffraction file (PDF))

Fig. 4. X-ray diffractograms of hardened FA/MKPC binders after exposure up to 1200 °C.

#75-1076) was identified as the main crystalline product in the FA/MKPC binder (Fig. 4). Traces of unreacted periclase (MgO, PDF #45-0946) with crystalline quartz (SiO₂, PDF #78-2315) and mullite (3Al₂O₃·2SiO₂, PDF #15-0776) from fly ash were also identified. After exposure at 400 °C (and air-cooling), the reflections associated with struvite-K disappeared in the FA/MKPC binder, and only reflections associated with periclase, quartz and mullite were observed. This was in agreement with previous work [33,44], which found that the long-range order of struvite-K collapsed after exposure to 200 °C *via* loss of the water of crystallisation. Although the long-range order was extensively disrupted, the physical integrity was retained in the blended MKPC binders, where no cracking, disintegration or distortion of the cylindrical shape was observed after exposure to 200–1200 °C (Fig. 2). At 400 °C, low intensity reflections indicative of orthorhombic MgKPO₄ were also observed (assignment based on data in [45]), which increased in relative intensity after exposure to 800 °C. There were no apparent changes associated with mullite and quartz reflections (present in the raw FA) up to 800 °C, which indicated that no fly ash reaction occurred at these temperatures, this was in agreement with Ding et al., who reported that no fly ash reaction would occur below 1000 °C [26].

In these *ex-situ* XRD measurements, the orthorhombic MgKPO₄ (β-MgKPO₄, *Pna2₁;* or γ-MgKPO₄, *Pnma*) polymorph (denoted as O-MgKPO₄ in Fig. 4) was observed at room temperature, which was in contrast to the literature based on pure MgKPO₄ [45,46] and struvite-K exposed to high temperature [44]. Monoclinic α-MgKPO₄ (*P2₁/c*) is the polymorph typically reported at room temperature, with reversible transitions observed to the orthorhombic forms on heating [44,46]. It is postulated that the presence of FA (source of Si, Al and Fe) altered the chemistry sufficiently to allow for the continued presence of orthorhombic MgKPO₄ during *ex-situ* analysis (rather than the room temperature polymorph, α-MgKPO₄). Further dissimilarities to struvite-K [44] (*i.e.* MKPC with no FA and GBFS) were observed after exposure to 1000 °C with the emergence of new crystalline reflections, which were associated with leucite (KAlSi₂O₆, PDF #38-1423). This was
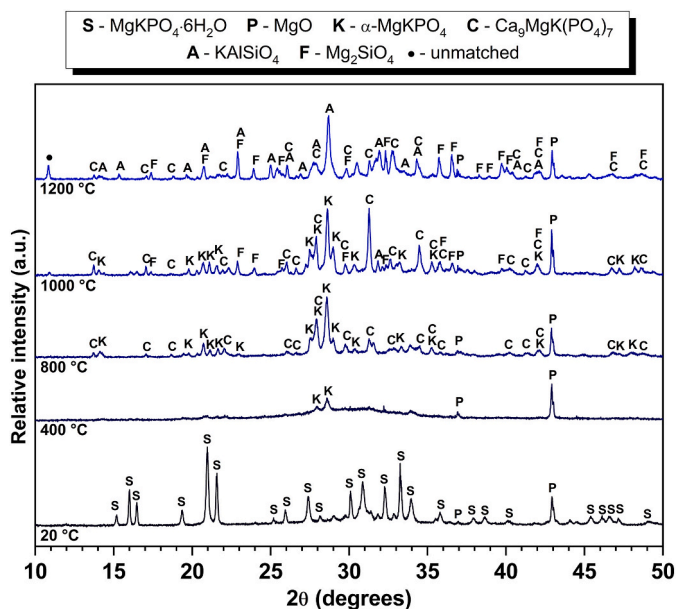
Fig. 5. X-ray diffractograms of hardened GBFS/MKPC binders after exposure up to 1200 °C.

indicative of a reaction between $MgKPO_4$ with the fly ash particles at this temperature, which did not occur in the high temperature struvite-K study due to the lack of a Si and Al source [44]. In FA/MKPC (Fig. 4), additional new phases at 1000 °C included $Mg_2P_2O_7$ (PDF #32-0626) and hematite (Fe_2O_3, PDF #33-0664). $Mg_2P_2O_7$ was observed in struvite-based ($NH_4MgPO_4 \cdot 6H_2O$) dental investments heated between 750 and 1100 °C [27,28] showing some similarities between the analogue system. It was also found in MKPC blended with wollastonite exposed to 800–1000 °C, where a combination of $Mg_2P_2O_7$ and $Mg_3(PO_4)_2$ phases were observed [32]. In Fig. 4, K was successfully retained within crystalline phases *via* $MgKPO_4$ – fly ash reactions, which is dissimilar to the cited studies, where K (or NH_3) was eliminated from the crystalline phases.

The chemistry of the FA/MKPC binder after exposure to 1200 °C appeared to favour the formation of leucite, as the relative intensity of the reflections increased compared to O-$MgKPO_4$, MgO and SiO_2, which correspondingly decreased. This indicated that further reaction occurred in the binder subjected to heat treatment at 1200 °C (*i.e.* more fly ash was reacting). This was reinforced by the formation of an iron-magnesium aluminate spinel phase similar to $Mg_1Al_{0.8}Fe_{1.2}O_4$ (PDF #71-1235), which was also observed in SEM/EDX analysis at this temperature (discussed further in Section 3.4.1) and the reduction in relative intensity of the quartz reflection at $2\theta = 26.6°$. A similar transition was observed in FA-derived geopolymers, where leucite was identified as the main crystalline product formed in a K-aluminosilicate binder after exposure to 1200 °C [47]. The melting point of $MgKPO_4$ was reported to be between 1404 °C [45] and 1520 °C [48], however, the MgO-K_2O-P_2O_5 ternary phase diagram indicates that small changes in the MgO content could reduce the melting point to <1300 °C [48]. As such, it is plausible to state that in the FA/MKPC sample exposed to 1200 °C, the observed reduction of $MgKPO_4$ reflections (Fig. 4) could be assigned to the formation of a $MgKPO_4$ vitrified phase, which did not recrystallise on cooling. The crystalline to glass transition was clearly incomplete at this temperature as remnant $MgKPO_4$ reflections remained.

3.2.2. GBFS/MKPC

At 20 °C, the diffraction pattern of the GBFS/MKPC binder (Fig. 5) identified struvite-K as the main crystalline phase. After exposure at 400 °C (and air-cooling), the main XRD response was a diffuse scattering feature between $25° < 2\theta < 35°$, which was assigned to the glassy slag fraction, along with low intensity reflections associated with the dehydrated phase, α-$MgKPO_4$, similar to the FA/MKPC binder at the same temperature. After exposure to 800 °C, α-$MgKPO_4$ (PDF #50-0146) was observed at room temperature, in agreement with the pure struvite-K system [44] but showing dissimilar behaviour to the FA/MKPC binder in Fig. 4. In addition, a calcium magnesium potassium phosphate phase ($Ca_9MgK(PO_4)_7$, PDF #88-0798) was observed, which is the K-bearing analogue for merrillite ($Ca_9NaMg(PO_4)_7$), a member of the whitlockite group. The presence of the latter phase indicates that there was a reaction between the slag particles (rich in Ca) and $MgKPO_4$ after exposure to 1000 °C.

For the GBFS/MKPC binder, after heat treatment at 1000 °C (Fig. 5), reflections associated with forsterite (Mg_2SiO_4, PDF #34-0189) emerged and the relative intensity of the $Ca_9MgK(PO_4)_7$ reflections increased. The identification of forsterite (Mg_2SiO_4) within the phase assemblage indicates that the slag particles have partially recrystallised after exposure at 1000 °C, in agreement with the work of Osborn et al. [49] who indicated that an equilibrium between forsterite, diopside, melilite and liquid could exist at 1250 °C for similar slag compositions. After exposure to 1200 °C, significant changes were observed in the phase assemblage indicative of an increased reaction between GBFS and $MgKPO_4$, which resulted in the emergence of kalsilite ($KAlSiO_4$, PDF #33-0989) as the prominent crystalline phase alongside increased forsterite contributions. It was expected that a vitrified phase was formed within the GBFS/MKPC binder after exposure to 1200 °C, due to the complete absence of $MgKPO_4$ reflections and reduced intensities of $Ca_9MgK(PO_4)_7$ reflections without the new Ca or P phases observed within the corresponding diffraction pattern.

3.3. Nuclear magnetic resonance spectroscopy

3.3.1. ^{27}Al MAS NMR

The ^{27}Al MAS NMR spectra for the FA/MKPC and GBFS/MKPC binders after exposure to temperature ranging between 20 and 1200 °C are shown in Fig. 6A–B. In the FA/MKPC binder (20 °C) two main Al environments, Al^{IV} and Al^{VI}, centred at 50 ppm and −3 ppm, respectively, were observed. The latter was assigned to the Al^{VI} sites in the mullite constituent of the fly ash [50,51], whilst the broad resonance centred at 50 ppm was assigned to a combination of the highly cross-linked aluminosilicate glassy fraction present in raw fly ash and tetrahedral mullite at 46 ppm [50]. No significant changes in the FA/MKPC binder were observed after exposure to 400 °C, however after heat treatment at 800 °C, the width and intensity of the Al^{IV} resonance (glassy fraction) increased whilst the intensity of the Al^{VI} resonance (assigned to mullite) appeared reduced. These spectral differences indicate that the Al environments present in fly ash changed as a result of exposure at these temperatures exposure but without Al incorporation into new crystalline phases.

After exposure to 1000 °C, the Al^{VI} resonance was almost entirely eliminated, and the Al^{IV} resonance changed to an asymmetric shape, comprised of three distinct, but overlapping, Al^{IV} environments centred at 68, 59, and 46 ppm, respectively. The latter was associated with a remnant fly ash environment suggesting an incomplete reaction occurred after exposure to 1000 °C. The resonances centred at 68 and 59 ppm are representative of leucite [52,53] and consistent with the XRD analysis (Fig. 4). After heat treatment at 1200 °C, the intensity of the
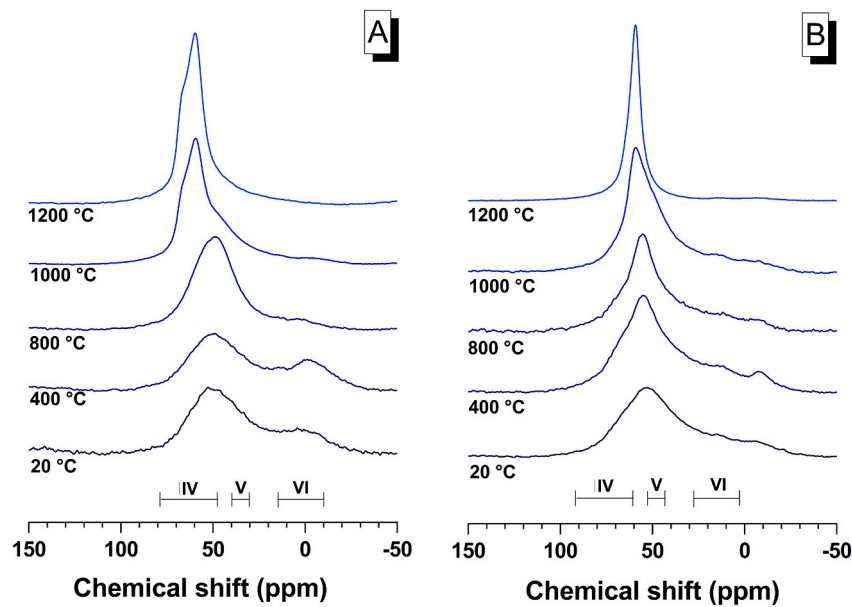
Fig. 6. ^{27}Al MAS NMR spectra of hardened A) FA/MKPC and B) GBFS/MKPC binders after exposure up to 1200 °C.
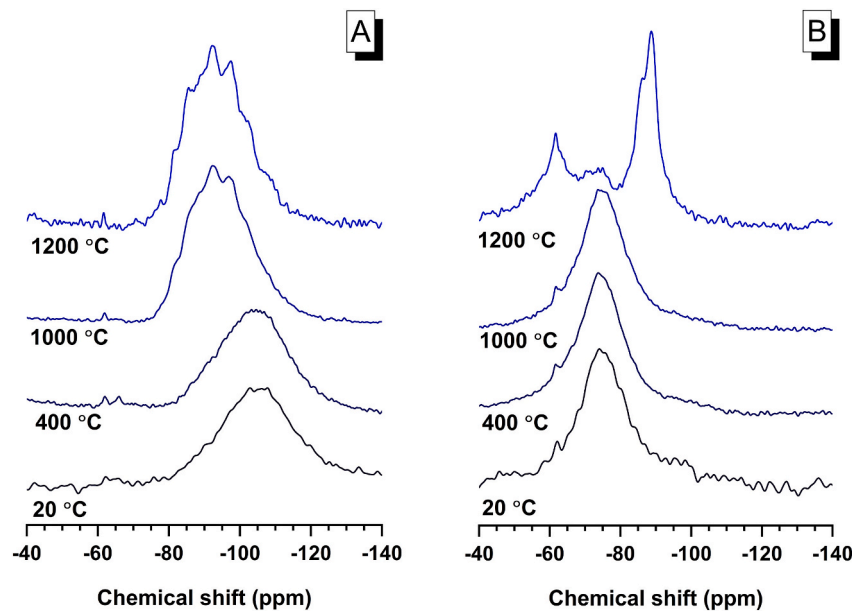

Fig. 7. ^{29}Si MAS NMR spectra of hardened A) FA/MKPC and B) GBFS/MKPC binders after exposure up to 1200 °C.

leucite resonances increased whereas the line width narrowed (compared to 1000 °C), with a notably reduced Al^{IV} contribution from the remnant fly ash. This was suggestive of a continued FA and MgKPO$_4$ reaction leading to additional leucite formation, which concurs with the observations in Fig. 4. The Mg$_1$Al$_{0.8}$Fe$_{1.2}$O$_4$ spinel observed *via* XRD analysis (Fig. 4; 1000 °C) could not be confidently assigned to a resonance(s) in the equivalent ^{27}Al MAS NMR spectrum (Fig. 6A; 1000 °C). MgAl$_2$O$_4$ spinels typically have two well resolved resonances at ~4 ppm and ~62 ppm representative of Al^{VI} and Al^{IV} environments, respectively (at 9.4 T), [54] however, these regions overlap with the dominant leucite / remnant fly ash contributions in Fig. 6A.

In Fig. 6B, the ^{27}Al MAS NMR spectrum of the GBFS/MKPC binder at 20 °C revealed the presence of two Al environments with the dominant site represented by a broad Al^{IV} environment centred at 53 ppm assigned

to the calcium aluminosilicate glass, which constitutes the majority of the slag [55]. Compared to the data for the raw slag reported previously [36], the main Al^{IV} resonance was narrower, slightly more intense and shifted upfield (centred at 53 ppm rather than 56 ppm) indicating a minor reaction of the slag during the hardening of the GBFS/MKPC binder. After exposure to temperatures between 400 and 1000 °C, a gradual downfield shift in the broad Al^{IV} resonance from 55 to 59 ppm was observed, along with increased asymmetry in the resonance shape, which was most notable after exposure to 1000 °C. This reorganization could be not assigned to the formation of new/additional Al crystalline phases within Fig. 5. In the GBFS/MKPC binder after exposure to 1200 °C, a single sharp Al^{IV} resonance was observed at 59.1 ppm (Fig. 6B) associated with the Q^4(4Si) units of an ordered kalsilite structure [56,57], which validated the assignment of a single Al-

containing phase within the XRD analysis (Fig. 5) and signalled that a solid state reaction between GBFS and MgKPO$_4$ had occurred within the GBFS/MKPC binder at this temperature.

3.3.2. ^{29}Si MAS NMR

The ^{29}Si MAS NMR spectra of the FA/MKPC and GBFS/MKPC binders exposed to temperatures between 20 and 1200 °C are shown in Fig. 7A–B. The FA/MKPC at 20 °C was found to have a broad resonance

Fig. 8. Backscattered electron micrographs and elemental maps of FA/MKPC binders after exposure to temperatures of; A) 20 °C, B) 1000 °C and C) 1200 °C.

between −76 and −122 ppm centred at −105 ppm (Fig. 7A), which was assigned to the crystalline and glassy aluminosilicate phases present: quartz ($\sim$−107 ppm) [58], mullite ($\sim$−86 ppm) [50], and the vitreous fraction [59]. After exposure at 400 °C, the resonance lineshape was similar to the FA/MKPC spectrum at 20 °C, indicating the continued presence of fly ash, whereas for the sample exposed to 1000 °C, the resonance shapes and chemical shifts of the partially resolved component peaks varied considerably. The component peaks identified at 1000 °C (at −86, −92 and −96 ppm) and 1200 °C (these same peaks plus additional resonances at −82 and −106 ppm) are consistent with leucite (KAlSi$_2$O$_6$) [60], as identified by XRD analysis (Fig. 4).

In Fig. 7B, the GBFS/MKPC (20 °C) was observed to have a broad resonance centred at −74 ppm, which was consistent with the dominant glassy fraction and the minor åkermanite present in the slag [61] and previous data, in addition to a minor resonance at −62 ppm that was attributed to a secondary siliceous reaction product [36]. After exposure to 400 °C and 1000 °C, no changes were observed in the ^{29}Si MAS NMR spectra, which indicated that the slag did not undergo significant reaction at these temperatures. After exposure at 1200 °C, the emergence of additional, sharp and intense resonances centred at −61.6, −86.2 and −88.8 ppm demonstrated that substantial reaction between GBFS and MgKPO$_4$ had taken place. However, the presence of a residual low intensity resonance at −73 ppm indicated that the slag reaction was incomplete at this temperature. The resonance at −61.6 ppm in Fig. 7B was attributed to forsterite (Mg$_2$SiO$_4$) [62,63], whilst the overlapping resonances at −88.9 and −86.2 ppm were thought to be a combination of an ordered kalsilite structure [56,57] and quenched-disordered kalsilite (transformation occurs at 897 °C), which is denoted as O1-KAlSiO$_4$ [64,65]. The spectra cited in those previous studies for a combination of quenched-disordered and ordered kalsilite are very similar to the ^{29}Si MAS NMR spectra reported here.

3.4. Scanning electron microscopy

The backscattered electron micrographs and elemental maps of FA/MKPC and GBFS/MKPC binders without thermal treatment are shown in Figs. 8A and 9A, respectively. The formation of a continuous struvite-K binder was observed, with larger struvite-K crystallites of this phase embedded in the continuous (and apparently microcrystalline) binder in both systems. Spherical particles of varying sizes and with high-contrast Fe-rich inclusions are associated with fly ash, whilst angular light grey particles are related to slag grains and the dark grey angular particles represent unreacted periclase. The following section describes the morphology and chemical distribution of phases in each blended MKPC binder after exposure at 1000 °C and 1200 °C.

3.4.1. FA/MKPC

After exposure to 1000 °C, the FA/MKPC binder appeared transformed from that typical of an MKPC binder (Fig. 8A) to a sintered yet porous matrix, with no distinct features associated with struvite-K and FA (Fig. 8B). Remnant fly ash particles were identifiable within the EDX maps (Fig. 8B: Al and Si) signalling that the FA reaction (observed by the formation of leucite, KAlSi$_2$O$_6$) was incomplete at this temperature. In Fig. 8B, a considerable distribution of Mg and P (with widespread K) was observed in the elemental maps for FA/MKPC binder after exposure to 1000 °C. The differences between the FA-rich and Mg/P rich regions were difficult to separate by contrast due to only a slight difference in grey scale, however EDX spectra (see supplementary data, Fig. S1) support the segregation of elements as described above. After heat treatment to 1000 °C, Fe migration was observed into rims around the MgO particles as well as forming discrete particles within the binder, which could be assigned to the emergence of hematite in Fig. 4 at this temperature.

After exposure to 1200 °C (Fig. 8C), remnant fly ash particles were no longer distinguishable from the bulk FA/MKPC binder, indicating additional FA/MgKPO$_4$ reactions occurred compared to 1000 °C, which
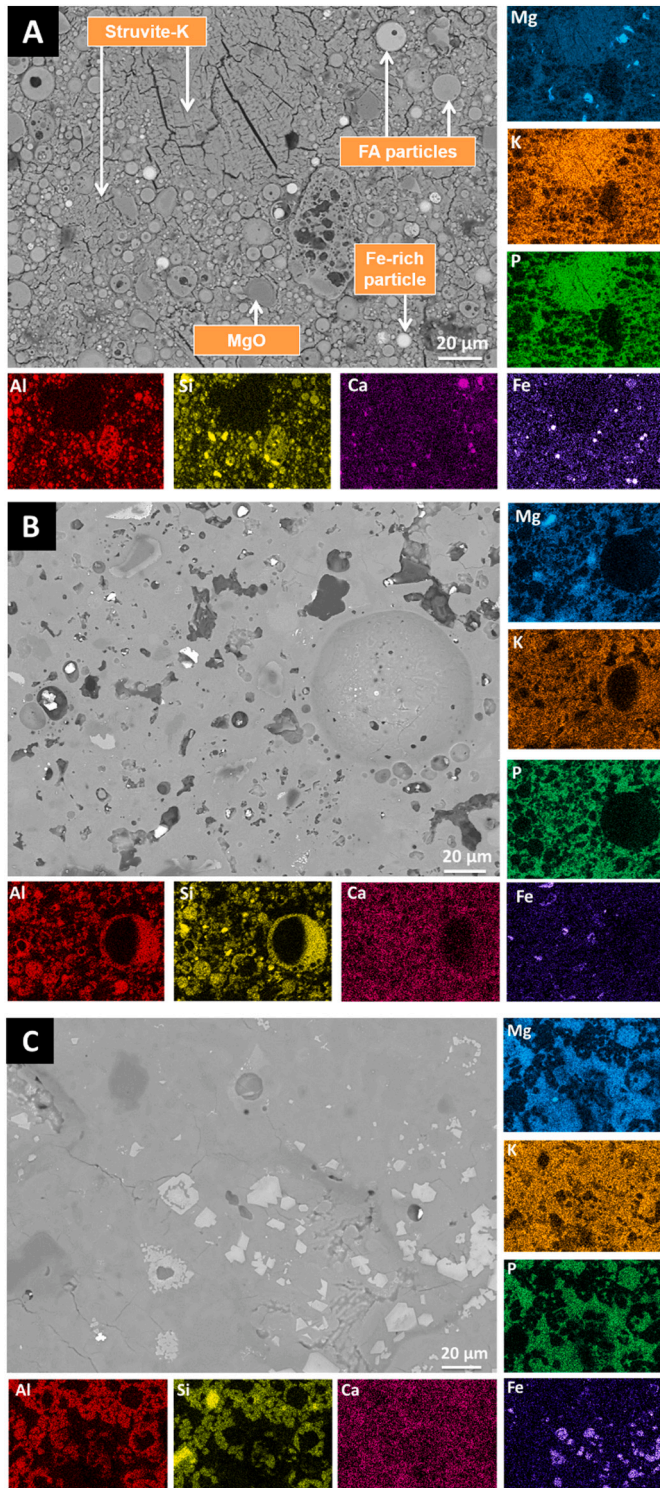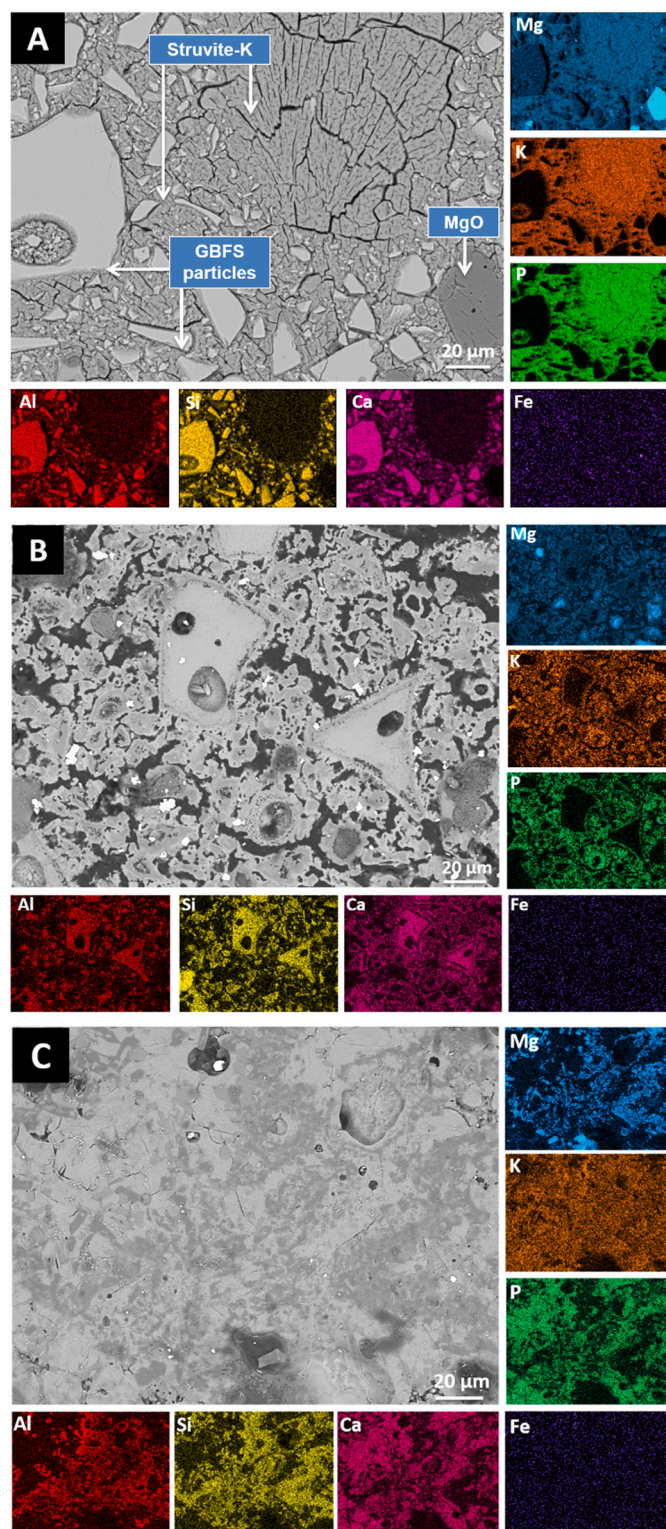
Fig. 9. Backscattered electron micrographs and elemental maps of GBFS/MKPC binders after exposure to temperatures of; A) 20 °C, B) 1000 °C and C) 1200 °C.

was supported by Mössbauer spectroscopy (Section 3.5). The visible porosity appeared reduced and a highly localised Fe-rich phase was observed. These changes are consistent with the XRD and NMR results. Again there was only a minor variance in BSE contrast (Fig. 8C) but the elemental maps (and spectra; see Fig. S2) revealed a continued elemental separation between the Al/Si and Mg/P rich regions within the sintered FA/MKPC sample. The bulk matrix can be assigned to both

$KAlSi_2O_6$ (Fig. 8C: Al, Si and K) and $MgKPO_4$ (likely to also include an $MgKPO_4$ melt phase as discussed earlier). Fe (Fig. 8C: Fe) was associated with the bright angular particles, which correspond to the spinel phase, $MgAl_{0.8}Fe_{1.2}O_4$. The actual composition of the spinel was calculated using SEM/EDX point analysis (based on 10 points) to have Al/Mg and Fe/Mg ratios of 0.71 ± 0.06 and 1.12 ± 0.35 (atomic %), respectively, which appears closely related to the XRD matched phase. A similar reaction pathway was observed by MacKenzie et al. [66] in a calcium silicate system containing Fe_2O_3 (10 wt%) where, after exposure to 1200 °C, $MgAl_2O_4$ was observed.

3.4.2. GBFS/MKPC

Differences were observed in the GBFS/MKPC binder after exposure to 1000 °C (Fig. 9B) when compared to the unexposed sample (Fig. 9A, 20 °C). The black areas in Fig. 9B are rich in C and O (maps not shown) indicative of resin impregnation of existing porosity during mounting for SEM analysis. From this observation, heat treatment to 1000 °C (but prior to the $MgKPO_4$ – GBFS reaction and formation of vitreous phases) resulted in elevated porosity compared to the GBFS/MKPC binder at 20 °C. In Fig. 9B, the angular slag particles and the dehydrated phase, α-$MgKPO_4$, continued to exist as a connected matrix interspersed with unreacted MgO. The elemental analysis revealed that the Al and Si remain associated with slag particles (*i.e.* minimal reaction beyond the extent seen at room temperature [36]) whereas, rims rich in Ca, Mg, K and P (Fig. 9B) were found on the larger slag particles that indicated migration of Ca to form the $Ca_9MgK(PO_4)_7$ phase identified in the XRD data (Fig. 5). The microstructure of GBFS/MKPC after exposure to 1000 °C was consistent with the XRD and NMR analysis (Figs. 5, 6B and 7B) but dissimilar to that of the FA/MKPC binder, where the sample appeared to have sintered with evidence of K migration, associated with the formation of leucite, $KAlSi_2O_6$.

After exposure to 1200 °C (Fig. 9C), the porosity appeared reduced with no visible slag particles (unlike after heat treatment to 1000 °C). Based on greyscale differences, the dark grey region, rich in Al, Si and Mg (Fig. 9C) represents a combination of kalsilite ($KAlSiO_4$) and forsterite (Mg_2SiO_4) whilst the light grey phase appears rich in Ca, K, and P. This region is likely associated with a combination of $Ca_9MgK(PO_4)_7$ and a calcium potassium phosphate glass phase of unknown composition (see Fig. S3). The latter is agreement with Fig. 5, where very few P-containing phases could be identified. Interestingly, the EDX maps in Fig. 9C reveal the apparent dissociation of Mg from P after exposure to 1200 °C, with Mg favouring the formation of silicate minerals and P preferentially associated with Ca (from GBFS). The SEM/EDX data in Fig. 9 supports the occurrence of a reaction between MKPC and GBFS, leading to the formation of potassium aluminosilicates, magnesium silicates, and calcium potassium phosphates, however the remnant slag environment identified in the ^{29}Si MAS NMR spectra (Fig. 7) could not be identified in Fig. 9C.

3.5. Mössbauer spectroscopy

Mössbauer spectroscopy was utilised to investigate Fe speciation in FA/MKPC binders exposed to high temperatures, data are shown in Fig. 10 for fly ash and FA/MKPC binders after heat treatments at 20, 800, 1000 and 1200 °C. Analysis of fly ash (Fig. 10A) indicated that both magnetic and non-magnetic fractions were present, in the form of hematite, magnetite and mullite (described as $3Al_2O_3 \cdot 2SiO_2$ but with Fe substitution for some of the Al [67]). Two doublets with isotropic shifts centred at 0.39 ± 0.02 and 0.78 ± 0.06 mm/s were associated with mullite, whilst the three sextets were associated with magnetic Fe species identified as hematite and magnetite. With increasing temperature (up to 1000 °C) preferential Fe oxidation, from Fe^{2+} to Fe^{3+}, was observed, which was consistent with the observed colour change (grey to red/brown, Fig. 2) and the emergence of hematite reflections in the corresponding XRD pattern in Fig. 4.

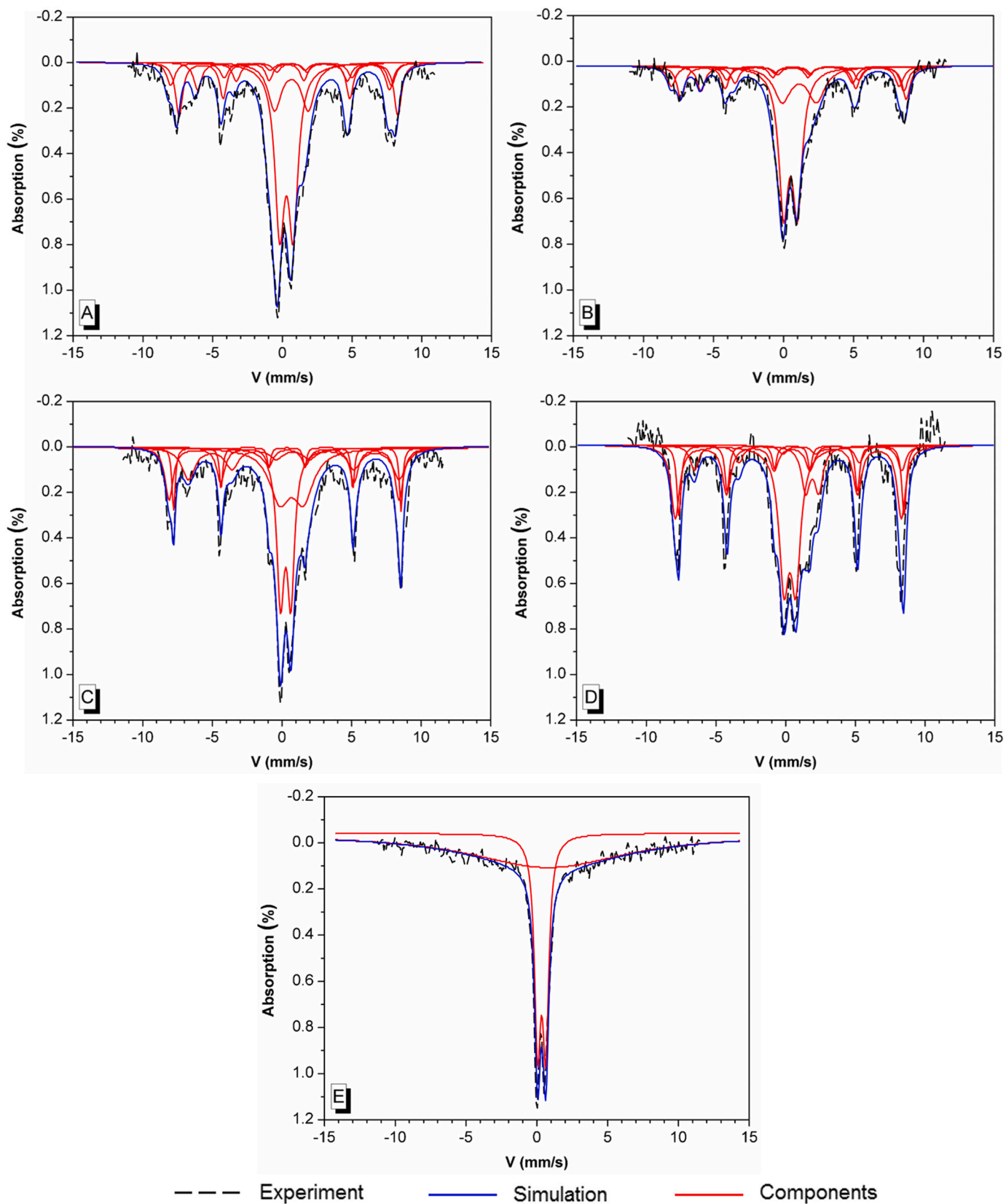After exposure to 1200 °C, a doublet signal was observed in the

Fig. 10. Mössbauer spectra of A) raw FA and FA/MKPC at; B) 20 °C and after exposure to C) 800 °C, D) 1000 °C and E) 1200 °C. The data are represented by the black points, whilst the simulations (blue) and simulation components (red) are represented by the solid lines. (For interpretation of the references to colour in this figure legend, the reader is referred to the web version of this article.)

Mössbauer spectrum rather than the sextuplets associated with magnetite and hematite (Fig. 10E). This was consistent with the presence of the spinel phase $MgAl_{0.8}Fe_{1.2}O_4$ identified by XRD and SEM/EDX analysis. A related spinel phase was observed by MacKenzie et al. [66] in kaolinite (aluminium silicate) systems containing Fe_2O_3 (10 wt%) where, after exposure to 1200 °C, $MgAl_2O_4$ was formed. No Mössbauer spectroscopy data were obtained for the GBFS/MKPC binder due to the low Fe content (0.4 wt%, Table 1).

4. Conclusions

In this study, FA/MKPC and GBFS/MKPC binders were exposed to a range of temperatures between 400 and 1200 °C to investigate the high temperature behaviour of these materials. After exposure to 400 °C, the dehydration of struvite-K ($MgKPO_4 \cdot 6H_2O$) to the dehydration product, $MgKPO_4$, was observed commensurate with the loss of long-range crystallographic order. At 800 °C, reflections associated with $MgKPO_4$ emerged for both systems in agreement with the high temperature behaviour of pure struvite-K. However, in the FA/MKPC and GBFS/MKPC binders exposed to 1000 and 1200 °C, respectively, a solid state reaction between fly ash/slag and $MgKPO_4$ occurred, resulting in the formation of the potassium aluminosilicate minerals; leucite and kalsilite, amongst other crystalline phases (hematite, spinel, forsterite). After heat treatment at temperatures above 1000 °C, very few crystalline phosphate compounds could be identified within the blended MKPC binders suggesting the likely formation of poorly crystalline phosphate-containing phases (e.g. vitreous phases). As a result of this evolution of the phase assemblage, considerable changes were observed in the microstructures of FA/MKPC and GBFS/MKPC binders after thermal treatment compared to binders at 20 °C. Although the phase assemblage and microstructure of FA/MKPC and GBFS/MKPC binders were considerably altered at high temperatures, they formed stable products whilst retaining physical stability with no evidence of spalling/cracking. This suggests that these systems could be expected to meet the fire performance requirements for UK conditioned intermediate level wastes which areassociated with the hazards of transport (withstanding exposure to a hydrocarbon fire at 800 °C for 30 min) [38] and geological disposal (withstanding exposure to a fire at 1000 °C for 60 min) [16] for specified types of nuclear waste. However, full-scale trials would be required to validate this statement prior to implementation within the nuclear industry, due to the relatively small specimens ($h = 10$ mm, $d = 14$ mm) utilised in this study.

CRediT authorship contribution statement

Laura J. Gardner: Writing – Original Draft, Methodology, Visualization, Formal analysis, Investigation

Sam A. Walling: Writing – Review and Editing, Formal analysis

Claire L. Corkhill: Writing – Review and Editing, Supervision, Methodology

Susan A. Bernal: Writing – Methodology, Review and Editing

Valentin Lejeune: Writing – Review and Editing, Formal analysis, Investigation, Methodology,

Martin C. Stennett: Writing – Review and Editing, Investigation

John L. Provis: Writing – Review and Editing

Neil C. Hyatt: Writing – Review and Editing, Supervision, Funding acquisition, Methodology

Declaration of competing interest

The authors declare that they have no known competing financial interests or personal relationships that could have appeared to influence the work reported in this paper.

Appendix A. Supplementary data

Supplementary data to this article can be found online at https://doi.org/10.1016/j.cemconres.2020.106332.

References

[1] S.A. Walling, J.L. Provis, Magnesia based cements – a journey of 150 years, and cements for the future? Chem. Rev. 116 (2016) 4170–4204.

[2] Z. Lai, H. Wang, Y. Hu, T. Yan, Z. Lu, S. Lv, H. Zhang, Rapid solidification of highly loaded high-level liquid wastes with magnesium phosphate cement, Ceram. Int. 45 (2019) 5050–5057.

[3] F. Qiao, C.K. Chau, Z. Li, Property evaluation of magnesium phosphate cement mortar as patch repair material, Constr. Build. Mater. 24 (2010) 695–700.

[4] L. Mo, L. Lv, M. Deng, J. Qian, Influence of fly ash and metakaolin on the microstructure and compressive strength of magnesium potassium phosphate cement pwaste, Cem. Concr. Res. 111 (2018) 116–129.

[5] A.S. Wagh, R. Strain, S.Y. Jeong, D. Reed, T. Krause, D. Singh, Stabilization of rocky flats Pu-contaminated ash within chemically bonded phosphate ceramics, J. Nucl. Mater. 265 (1999) 295–307.

[6] S.E. Vinokurov, Y.M. Kulyako, O.M. Slyuntchev, S.I. Rovny, B.F. Myasoedov, Low-temperature immobilization of actinides and other components of high-level waste in magnesium potassium phosphate matrices, J. Nucl. Mater. 385 (2009) 189–192.

[7] A.S. Wagh, S.Y. Sayenko, V.A. Shkuropatenko, R.V. Tarasov, M.P. Dykiy, Y. O. Svitlychniy, V.D. Virych, E.A. Ulybkina, Experimental study on cesium immobilization in struvite structures, J. Hazard. Mater. 302 (2016) 241–249.

[8] E. Banks, R. Chianelli, R. Korenstein, Crystal chemistry of struvite analogs of the type $MgMPO_4 \cdot 6H_2O$ ($M^+ = K^+$, Rb^+, Cs^+, Tl^+, NH_4^+), Inorg. Chem. 14 (1975) 1634–1639.

[9] J.H. Sharp, N.B. Milestone, J. Hill, E.W. Miller, Cementitious systems for encapsulation of intermediate level waste, in: The 9th International Conference on Radioactive Waste Management and Environmental RemediationOxford, UK, 2003.

[10] N.B. Milestone, Reactions in cement encapsulated nuclear wastes: need for toolbox of different cement types, Adv. Appl. Ceram. 105 (2006) 13–20.

[11] M. Hayes, I.H. Godfrey, Development of the use of alternative cements for the treatment of intermediate level waste, in: Waste Management Symposia Proccedings AZ, USA, 2007, pp. 1–14.

[12] A. Covill, N.C. Hyatt, J. Hill, N.C. Collier, Development of magnesium phosphate cements for encapsulation of radioactive waste, Adv. Appl. Ceram. 110 (2011) 151–156.

[13] C. Cau Dit Coumes, D. Lambertin, H. Lahalle, P. Antonucci, C. Cannes, S. Delpech, Selection of a mineral binder with potentialities for the stabilization/solidification of aluminum metal, J. Nucl. Mater. 453 (2014) 31–40.

[14] C. Paraskevoulakos, C.A. Stitt, K.R. Hallam, A. Banos, M. Leal Olloqui, C.P. Jones, G. Griffiths, A.M. Adamska, J. Jowsey, T.B. Scott, Monitoring the degradation of nuclear waste packages induced by interior metallic corrosion using synchrotron X-ray tomography, Constr. Build. Mater. 215 (2019) 90–103.

[15] Nuclear Decommissioning Authority, Geological disposal: Gas status report NDA/RWMD/037, 2010, pp. 139.

[16] Nuclear Decommissioning Authority, Geological Disposal: Waste package accident performance status report, NDA/RWMD/032, 2010.

[17] Nuclear Decommissioning Authority, Waste package specification and guidance documentation; WPS/300/02, specification for 500 litre drum waste package, Nuclear Decommissioning Authority, 2008.

[18] U.S Department of Energy, Waste isolation pilot plant recovery plan, revision 0, 2014.

[19] F. Delhomme, J. Ambroise, A. Limam, Effects of high temperatures on mortar specimens containing Portland cement and GGBFS, Mater. Struct. 45 (2012) 1685–1692.

[20] D. Matesová, D. Bonen, S. Shah, Factors affecting the resistance of cementitious materials at high temperatures and medium heating rates, Mater. Struct. 39 (2006) 455–469.

[21] W.D. Kingery, Fundamental study of phosphate bonding in refractories: I, literature review, J. Am. Ceram. Soc. 33 (1950) 239–241.

[22] R.W. Limes, D. Ponzani, Basic refractory compositions for intermediate temperature zones, US Patent, 3285758 (1966).

[23] R.W. Limes, R.O. Russell, Process for preparing fast-setting aggregate compositions and products for low porosity produced therewith, US Patent, 3879209 (1975).

[24] N.E. Hipedinger, A.N. Scian, E.F. Aglietti, Magnesia–ammonium phosphate-bonded cordierite refractory castables: phase evolution on heating and mechanical properties, Cem. Concr. Res. 34 (2004) 157–164.

[25] Y. Fang, P. Cui, Z. Ding, J.-X. Zhu, Properties of a magnesium phosphate cement-based fire-retardant coating containing glass fiber or glass fiber powder, Constr. Build. Mater. 162 (2018) 553–560.

[26] Z. Ding, M.-R. Xu, J.-G. Dai, B.-Q. Dong, M.-J. Zhang, S.-X. Hong, F. Xing, Strengthening concrete using phosphate cement-based fiber-reinforced inorganic composites for improved fire resistance, Constr. Build. Mater. 212 (2019) 755–764.

[27] R. Neiman, A.C. Sarma, Setting and thermal reactions of phosphate investments, J. Dent. Res. 59 (1980) 1478–1485.

[28] T. Sugama, L.E. Kukacka, Magnesium monophosphate cements derived from diammonium phosphate solutions, Cem. Concr. Res. 13 (1983) 407–416.

[29] B. Xu, B. Lothenbach, H. Ma, Properties of fly ash blended magnesium potassium phosphate mortars: effect of the ratio between fly ash and magnesia, Cem. Concr. Compos. 90 (2018) 169–177.

[30] Y. Li, T. Shi, J. Li, Effects of fly ash and quartz sand on water-resistance and salt-resistance of magnesium phosphate cement, Constr. Build. Mater. 105 (2016) 384–390.

[31] Y. Li, T. Shi, B. Chen, Y. Li, Performance of magnesium phosphate cement at elevated temperatures, Constr. Build. Mater. 91 (2015) 126–132.

[32] X. Gao, A. Zhang, S. Li, B. Sun, L. Zhang, The resistance to high temperature of magnesia phosphate cement paste containing wollastonite, Mater. Struct. 49 (2016) 3423–3434.

[33] L.J. Gardner, V. Lejeune, C.L. Corkhill, S.A. Bernal, J.L. Provis, M.C. Stennett, N. C. Hyatt, Evolution of the phase assemblage in magnesium potassium phosphate cement binders at 200 and 1000 °C, Adv. Appl. Ceram. 114 (2015) 386–392.

[34] British Standard, Fly ash for concrete. Part 1: Definition, specifications and conformity criteria, BS EN 450–1, (2012).

[35] R.A. Sanderson, G.M. Cann, J.L. Provis, The effect of blast-furnace slag particle size on the hydration of slag–Portland cement grouts at elevated temperatures, Adv. Cem. Res. 30 (2017) 337–344.

[36] L.J. Gardner, S.A. Bernal, S.A. Walling, C.L. Corkhill, J.L. Provis, N.C. Hyatt, Characterisation of magnesium potassium phosphate cements blended with fly ash and blast furnace slag, Cem. Concr. Res. 74 (2015) 78–87.

[37] W. Montague, M. Hayes, L.J. Vandeperre, Strength - formulations correlations in magnesium phosphate cements for nuclear waste encapsulation in: H.-T. Lin, Y. Katoh, A.b. Vomiero (Eds.) The American Ceramic Society's 37th International Conference on Advanced Ceramics and Composites John Wiley & Sons, FL, USA, 2014, pp. 107–117.

[38] International Atomic Energy Agency, Advisory material for the IAEA regulations for the safe transport of radioactive material; 2012 edition, specific safety guide No. SSG-26, Vienna, 2014.

[39] K. Lagarec, D.G. Rancourt, Recoil - Mössbauer spectral analysis software for Windows, version 1.02, Department of Physics, University of Ottawa, Ottawa, (1998).

[40] E. Lang, Blastfurnace cements, in: J. Bensted, P. Barnes (Eds.), Structure and Performance of Cements, Spon Press, London, UK, 2002, pp. 310–325.

[41] H. Ma, B. Xu, Z. Li, Magnesium potassium phosphate cement paste: degree of reaction, porosity and pore structure, Cem. Concr. Res. 65 (2014) 96–104.

[42] L. Chong, J. Yang, C. Shi, Effect of curing regime on water resistance of magnesium–potassium phosphate cement, Constr. Build. Mater. 151 (2017) 43–51.

[43] L.J. Gardner, C.L. Corkhill, S.A. Walling, S.A. Bernal, J.E. Vigor, C.A. Murray, C. C. Tang, J.L. Provis, N.C. Hyatt, Early age hydration and aplication of blended magneisum potassium phosphate cements for reduced corrosion of reactive metals, Accepted, Cem. Concr. Res, 2021.

[44] L.J. Gardner, S.A. Walling, S.M. Lawson, C.L. Corkhill, S.A. Bernal, J.L. Provis, N. C. Hyatt, Characterization of and structural insight into struvite-K, MgKPO$_4$·6H$_2$O, an analogue of struvite, Inorganic Chemistry, 2020. In press.

[45] G. Wallez, C. Colbeau-Justin, T. Le Mercier, M. Quarton, F. Robert, Crystal chemistry and polymorphism of potassium–magnesium monophosphate, J. Solid State Chem. 136 (1998) 175–180.

[46] L. Miladi, A. Oueslati, K. Guidara, Phase transition, conduction mechanism and modulus study of KMgPO$_4$ compound, RSC Adv. 6 (2016) 83280–83287.

[47] T. Bakharev, Thermal behaviour of geopolymers prepared using class F fly ash and elevated temperature curing, Cem. Concr. Res. 36 (2006) 1134–1147.

[48] E. Lindström, M. Sandström, D. Boström, M. Öhman, Slagging characteristics during combustion of cereal grains rich in phosphorus, Energy Fuel 21 (2007) 710–717.

[49] E.F. Osborn, K.H. Gee, A. Muan, P.L. Roeder, G.C. Ulmer, Studies of phase equilbria in the systems: CaO - MgO- Al$_2$O$_3$ - SiO$_2$ and CaO - MgO- Al$_2$O$_3$ - TiO$_2$ - SiO$_2$, in: Bulletin of the Earth and Mineral Sciences Experiment Station 85, 1969, pp. 1–80.

[50] L.H. Merwin, A. Sebald, H. Rager, H. Schneider, ^{29}Si and ^{27}Al MAS NMR spectroscopy of mullite, Phys. Chem. Miner. 18 (1991) 47–52.

[51] H. He, J. Guo, J. Zhu, P. Yuan, C. Hu, ^{29}Si and ^{27}Al MAS NMR spectra of mullites from different kaolinites, Spectrochim. Acta A Mol. Biomol. Spectrosc. 60 (2004) 1061–1064.

[52] B.L. Phillips, R.J. Kirkpatrick, Short-range Si-Al order in leucite and analcime: determination of the configurational entropy from ^{27}Al and variable-temperature ^{29}Si NMR spectroscopy of leucite, its Cs and Rb-exchanged derivatives, and analcime, Am. Mineral. 79 (1994) 1025–1031.

[53] B.L. Phillips, R.J. Kirkpatrick, A. Putnis, Si,Al ordering in leucite by high-resolution ^{27}Al MAS NMR spectroscopy, Phys. Chem. Miner. 16 (1989) 591–598.

[54] D. Madej, K. Tyrała, In Situ Spinel Formation in a Smart Nano-Structured Matrix for No-Cement Refractory Castables, Materials (Basel);, 13 (2020).

[55] R.J. Kirkpatrick, MAS NMR spectroscopy of minerals and glasses, in: Spectroscopic Methods in Mineralogy and Geology, 1988, pp. 341–403. The Society.

[56] A.I. Becerro, M. Mantovani, A. Escudero, Hydrothermal synthesis of kalsilite: a simple and economical method, J. Am. Ceram. Soc. 92 (2009) 2204–2206.

[57] G.L. Hovis, D.R. Spearing, J.F. Stebbins, J. Roux, A. Clare, X-ray powder diffraction and ^{23}Na, ^{27}Al, and ^{29}Si MAS-NMR investigation of nepheline-kalsilite crystalline solutions, Am. Mineral. 77 (1992) 19–29.

[58] E. Lippmaa, M. Mägi, A. Samoson, G. Engelhardt, A.R. Grimmer, Structural studies of silicates by solid-state high-resolution ^{29}Si NMR, J. Am. Chem. Soc. 102 (1980) 4889–4893.

[59] Á. Palomo, S. Alonso, A. Fernandez-Jiménez, I. Sobrados, J. Sanz, Alkaline activation of fly ashes: NMR study of the reaction products, J. Am. Ceram. Soc. 87 (2004) 1141–1145.

[60] I.W.M. Brown, C.M. Cardile, K.J.D. MacKenzie, M.J. Ryan, R.H. Meinhold, Natural and synthetic leucites studied by solid state 29-Si and 27-Al NMR and 57-Fe Mossbauer spectroscopy, Phys. Chem. Miner. 15 (1987) 78–83.

[61] L.H. Merwin, A. Sebald, F. Seifert, The incommensurate-commensurate phase transition in akermanite, Ca$_2$MgSi$_2$O$_7$, observed by in-situ ^{29}Si MAS NMR spectroscopy, Phys. Chem. Miner. 16 (1989) 752–756.

[62] J.A. Tangeman, B.L. Phillips, A. Navrotsky, J.K.R. Weber, A.D. Hixson, T.S. Key, Vitreous forsterite (Mg$_2$SiO$_4$): synthesis, structure, and thermochemistry, Geophys. Res. Lett. 28 (2001) 2517–2520.

[63] M. Mägi, E. Lippmaa, A. Samoson, G. Engelhardt, A.R. Grimmer, Solid-state high-resolution silicon-29 chemical shifts in silicates, J. Phys. Chem. 88 (1984) 1518–1522.

[64] J.F. Stebbins, J.B. Murdoch, I.S.E. Carmichael, A. Pines, Defects and short-range order in nepheline group minerals: a silicon-29 nuclear magnetic resonance study, Phys. Chem. Miner. 13 (1986) 371–381.

[65] J.V. Smith, O.F. Tuttle, The nepheline-kalsilite system; part I, X-ray data for the crystalline phases, Am. J. Sci. 255 (1957) 282–305.

[66] K.J.D. MacKenzie, M.E. Bowden, The evolution of an unusual superparamagnetic Mössbauer resonance in iron-containing oxide and silicate systems, J. Mater. Sci. Lett. 2 (1983) 317–324.

[67] S. Gomes, M. François, M. Abdelmoula, P. Refait, C. Pellissier, O. Evrard, Characterization of magnetite in silico-aluminous fly ash by SEM, TEM, XRD, magnetic susceptibility, and Mössbauer spectroscopy, Cem. Concr. Res. 29 (1999) 1705–1711.

[68] N.C. Hyatt, C.L. Corkhill, M.C. Stennett, R.J. Hand, L.J. Gardner, C.L. Thorpe, The HADES facility for high activity decommissioning engineering & science: part of the UK national nuclear user facility, in: IOP Conference Proceedings: Materials Science and Engineering 818, 2020, 012022.